



# Generating High-Resolution Chest X-ray Images Using CGAN

Haneen M. Mohammed\*, Khawla H. Ali

Department of Computer Science, College of Education for Pure Science, University of Basrah, Basrah, Iraq.

## ARTICLE INFO

Received 05 August 2022  
Accepted 21 September 2022  
Published 30 December 2022

## Keywords :

COVID-19, Generative Adversarial Network, Conditional Generative Adversarial Network, Synthetic image

**Citation:** H.M. Mohammed, K.H. Ali, J. Basrah Res. (Sci.) **48**(2), 88 (2022).  
[DOI:https://doi.org/10.56714/bjrs.48.2.9](https://doi.org/10.56714/bjrs.48.2.9)

## ABSTRACT

Deep Learning (DL) models have outperformed remarkably and effectively on several Computers Vision applications. However, these models require large amounts of data to avoid overfitting problems. Overfitting happens when a network trains a function with an incredibly high variance to represent the training data perfectly. Consequently, medical images lack to availability of large labeled datasets, and the annotation of medical images is expensive and time-consuming for experts, as the COVID-19 virus is an infectious disease, these datasets are scarce and it is difficult to get large datasets. The limited amount of the COVID-19 class compared to any other classes, for example (healthy). To solve the scarcity data problem, we adjust a Conditional Generative Adversarial Network (CGAN) as a solution to the problems of scarcity and limited data. CGAN contains two neural networks: a generator that creates synthetic (fake) images, and a discriminator that recognizes a real sample of training and a generated sample from the generator. The adjusted CGAN is able to Generate synthetic images with high resolution and close to the original images which aid in expanding the limited dataset specific to a new pandemic. In addition to CGAN augmenting strategies, this research also briefly explores additional aspects of data augmentation like time augmentation and total dataset size. Frechet inception distance metric (FID) has been used for evaluating synthetic images generated by CGAN. The adjusted CGAN obtains better FID results for the high-resolution synthetic X-rays images it achieves 2.349%.

## 1. Introduction

The medical image field plays an essential role in various clinical applications, like medical procedures employed in the early detection, diagnosis, monitoring, and treatment evaluation of different medical conditions, that are used to investigate the internal functioning of the human body to perform medical diagnoses [1]. Recently, the DL approach has played an essential role in classifying and diagnosing medical images based on X-rays, Computed Tomography scanning (CT), and Magnetic Resonance Imaging (MRI), DL model learns the classification tasks directly, where the DL model can achieve an accuracy that exceeds the level of human performance, several DL models have been used to diagnose medical images [2].

Chest diseases are among the most critical health problems people face; for example, Coronavirus is a viral disease associated with Coronavirus2 (SARS-CoV-2), which attacks the respiratory system and

\*Corresponding author email : [hneenaltmemi@gmail.com](mailto:hneenaltmemi@gmail.com)



leads to severe acute respiratory syndrome. This virus leads to pneumonia, an infection that leads to inflammation of the air sacs in the lungs. In 2019, the disease first appeared in China; then, the infection quickly spread worldwide [3]. Due to the disease being highly contagious, the infected must be diagnosed and isolated quickly, as many techniques have emerged to detect the condition based on medical images, such as X-ray and CT scans image [4]. The detection of COVID-19s at an early may aid in controlling the disease's spread and containment.

However, there are still many challenges for the DL model to be completely reliable. One of the significant challenges is medical image scarcity; it is difficult to get large datasets due to the patient's privacy and this disease is highly contagious. Therefore, the medical image dataset is unbalanced and lacks available large labeled datasets that cause overfitting problems and lack generalization. The augmentation technique addresses the overfitting issue; then increases the diagnosis process's reliability and safety [5]. Data augmentation is often performed on training data to expand the size of the training set. We propose Generative Adversarial Networks (GANs) to artificially augment the dataset [6]. Especially Conditional Generative Adversarial Networks (CGANs), which create artificial instances retaining similar characteristics to the original dataset. CGAN is a particular type of standard GAN that can generate synthetic invisible COVID-19 X-ray images by learning the distribution of data from the actual data set based on the given class label [7]. We adjusted the CGAN augmentation method to augment the COVID-19 dataset.

The contribution of this paper is as follows:

- Utilized the CGAN augmentation technique effectively to increase the X-ray COVID-19 dataset, a safe and efficient method of collecting the COVID-19 dataset in a short time.
- Generated new images with high resolution and very close to the original images which aid in expanding the limited dataset specific to a new pandemic
- Solved unbalancing dataset issue by utilizing CGAN-based synthetic data, which can balance the two classes (COVID-19, normal) in the dataset and overcome the overfitting issue.
- Elaborated on the possible hyperparameters setting to adjust CGAN to produce the synthetic image in terms of quality and diversity.

The remainder of the work is divided into the following: a review of the related work in section 2. In section 3, the reader can find a detailed description of the data used and the proposed model of the considered networks. In section 4, results are presented and discussed. Finally, Chapter 5 contains a conclusion of the achievements of this paper and a description of possible future employment.

## 2. Related Works

Receive continued to develop in medical research, especially those interested in Synthetic data generation. Realistically-looking medical images have been proposed in healthcare to increase the diversity and quantity of current training data and improve the robustness of DL models. DL has recently impacted several scientific domains [8]. We reviewed some of the recent works to see which strategies were the most beneficial and progressed in the most previous studies. Over the last few decades, the research used in the medical field to categorize diseases has increased, showing an increasing demand for this field of study, which is still ongoing. Researchers have investigated techniques to increase datasets, Goodfellow et al. [9] published the first paper on GANs, which generate new synthetic images. As shown in Fig. 1, there has been an increase in publications using the search term "GAN" according to google scholar since the middle of 2020.

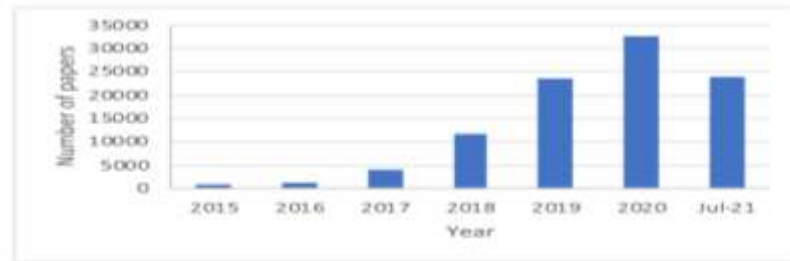


**Fig. 1.** A chart depicting the number of GAN papers published [10].

Salome Kazeminia et al. [11] published a survey about GAN for medical applications. This survey summarizes the utilized GAN for medical image processing applications such as segmentation, synthesis, reconstruction detection, de-noising, classification, and registration by the article's authors. Kohlberger et al. [12] synthesize pathology images for cancer with natural out-of-focus characteristics to assess general pathology images for focus quality issues. Likun Cai et al. [13] propose a novel value function for GAN framework using the alpha divergence which can be regarded as a generalization of the Kullback–Leibler divergence to improve Wasserstein-GAN based on three datasets MNIST, SVHN, and CeLebA. The objective introduces two more hyper-parameters to keep a balance during the Entropy of the training procedure and conduct a theoretical analysis for selecting appropriate hyper-parameters. Berezhsky et al. [14] present conditional Deep Convolution GAN-particle swarm optimization (cDCGAN-PSO), a version of algorithm of GANs to generate chest X-rays images. cDCGANs can synthesize multiple classes from X-rays images, the limitation is the number of generated images is limited which generates only 600 images for the COVID-19 class.

Konstantin Shmelkov. [15] This paper presents steps towards addressing the challenging problem of evaluating and comparing images generated by Wasserstein GAN (WGAN), Spectrally Normalized GAN (SNGAN), and Deep Convolution GAN (DCGAN). they present new quantitative measures, GAN-train and GAN-test. GAN-generated images on the CIFAR10 and CIFAR100 datasets respectively, the limitation is the generated images with low quality. shuang et al. [16] propose a new method for generating security synthetic X-ray images with multiple prohibited items from semantic label images based on Self-Attention GAN (SAGAN), a model is used to generate a large number of single-object semantic label images with various postures from random noise. Theoretically, they can use it to synthesize as many X-ray images as needed. A new generator architecture with Res2Net is presented, which is more effective in learning multi-scale features of different prohibited item images. This method is extended by establishing the semantic label library which contains 14000 images. Abdul Waheed et al. [17] Employed the Auxiliary Classifier GAN (ACGAN) to generate X-ray images for COVID-19. They chose 403 for the Covid-19 images and 721 for the normal images. They use the VGG16 model trained on the original and augmented data sets. They apply fine-tuning to adjust the parameter of the pre-trained VGG-16 model. So that it can adapt to the new task at hand. ACGAN only generates 1,399 images for normal cases and 1,669 images for COVID-19 patients. The limitations are low diagnostic accuracy due to the low resolution of the generated image, which takes five hours to generate synthetic images. Loey et al. [18] applied GAN with conventional augmentation on chest X-ray images to further distinguish four types of classes. The classes are the covid, normal, pneumonia bacterial, and pneumonia virus. They selected 307 images for each class. GAN with conventional augmentation generates synthetic images. The limitation is the generated images have low quality and limited diversification.

### 3. The Proposed Method

In this section, we present generated COVID-19 X-rays images based on four phases: setup phase, Image pre-processing phase, image augmentation phase, and evaluation phase. Fig. 2 shows the proposed method to extend the COVID-19 ray images dataset.

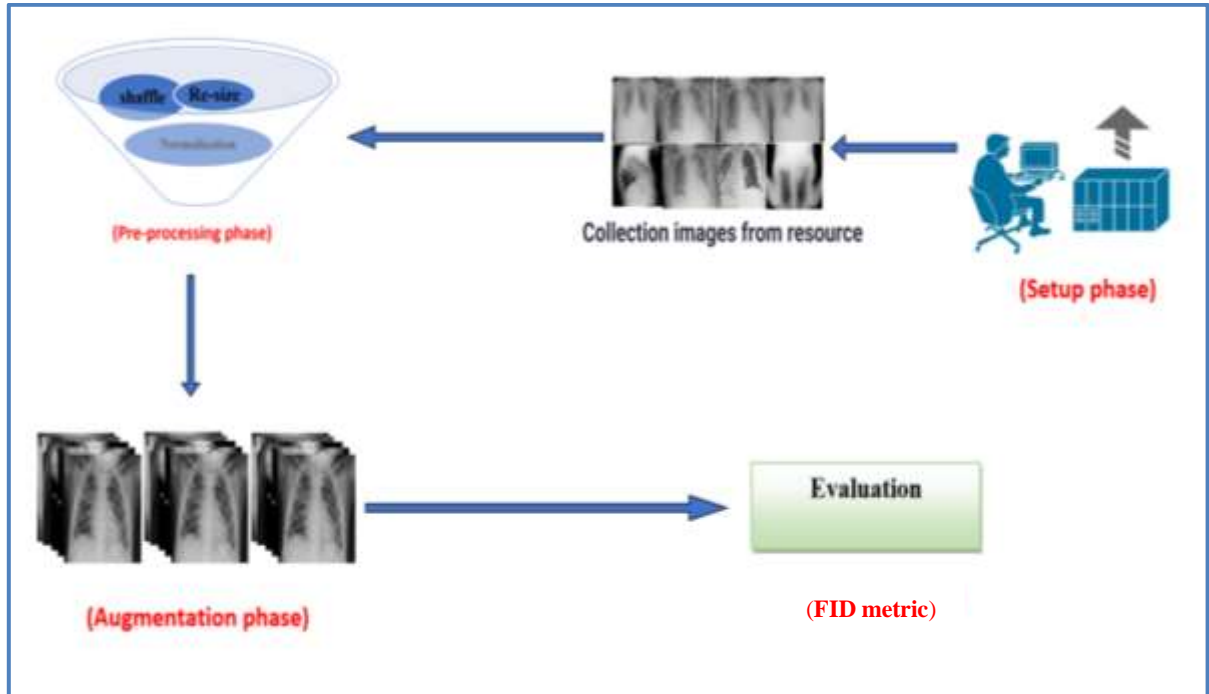


Fig. 2. The four stages for the generated COVID-19 X-rays images.

#### a. Setup Phase (Dataset’s Collection)

This section discusses the publicly available benchmark collection dataset utilized in our experiments. There are two-class datasets, the normal class for healthy people and the COVID-19 class for patients. The steps of collecting the dataset from its different resources until uploading it to its own Google Drive shows in Fig. 3.

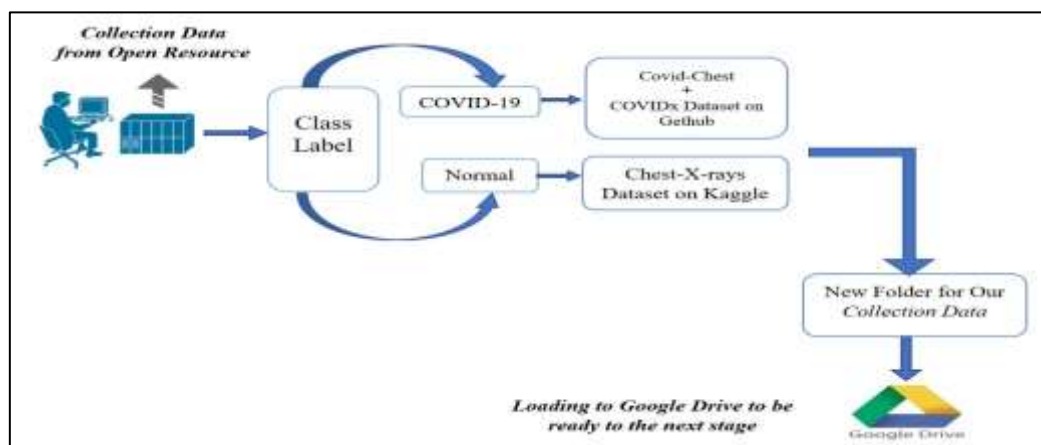


Fig. 3. The Main Steps for collecting our dataset.

The COVID-19 X-ray images are not widely available; we have collected COVID-19 images from various datasets. We utilized an available online chest X-ray collection. The first source of COVID-19 X-rays images is Covid-Chest-Dataset, published by Joseph Cohen et al. [19], which is publicly available on GitHub. New X-ray images continually update this dataset; the dataset contains 673 X-rays with different views and 349 CT scan images from patients affected by COVID-19 and other diseases, additionally other data about patients, such as age and sex in the metadata file. Another source of COVID-19 images was published by Wang et al. [20]. They used the covid-chest X-ray dataset and four publicly available datasets and compiled the COVIDx dataset. The COVIDx dataset contains 617 X-ray images for COVID-19 positive cases, the two COVID-19 datasets are merged. The normal dataset for our experiments is the chest X-rays dataset from the Kaggle [21]. This standard dataset consists of 1587 normal images, the collected dataset is stored in a new folder and loading in our Google Drive to be ready for the next stage. A detail of the collected dataset can be found in Table 1.

**Table 1.** The dataset that was utilized in this paper

Dataset Title	Classes	
	COVID-19	Normal
Covid-Chest-Dataset	673	0
COVID-Net	617	0
Chest-X-rays Dataset	0	1587

#### b. Pre-Processing Phase

Collected X-ray images were taken from the many public datasets with different image sizes, types, and resolutions. In this section, the pre-processing stage conations steps over the selected data sowed in Fig. 4.

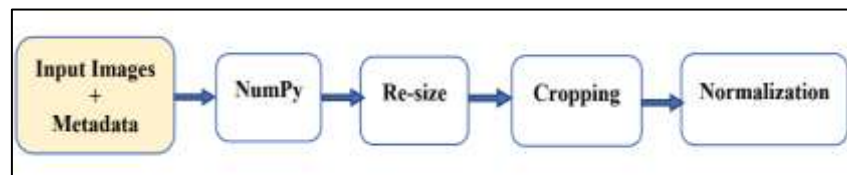


**Fig. 4.** The sequence operations for pre-processing Stage.

##### i. Convert to NumPy

The collected X-rays images were saved in 24-bit depth formats and various sizes, with the highest resolution being  $5623 \times 4757$ . To be easy to process each pixel in the medical image, we must convert it to a multi-dimensional array. NumPy is a popular Python library. It performs operations on multidimensional arrays and matrices and uses industry array computing for high-level mathematical functions.

##### ii. Resize Images

The image size changed according to the selected experiment. The resize process decreases the training time by reducing the number of pixels all images resize to  $224 \times 224$  pixels.

iii. Image Cropping

The radiation images in the collection differ in organ size, structural design, and human textures. This difference may make it difficult to detect diseases and waste time in the DL diagnostic approach. The model focuses on the chest for the diagnosis of chest diseases. there is no need for the remainder of the body's components, such as the neck or belly, these features increase training time and decrease training accuracy. The image cropping applies manually.

iv. Image Normalization

It is used to alter the pixel range of intensity values, making the image more palatable to the senses. Image batch normalization is frequently used to increase contrast, which benefits increased feature extraction tasks.

c. Augmentation phase

Image augmentation is a popular technique for improving the generalization capabilities of deep neural networks and avoiding overfitting due to a lack of training data in the medical image field. Image augmentation is useful for improving the performances of DL models [22].

i. Conditional Generative Adversarial Networks (CGAN)

GAN can generate synthetic random plausible examples for a target dataset, there is no method to determine the types of generated images. The conditional generative adversarial network CGAN is a version of the traditional GAN, it can be described as a training framework for Generative Artificial Neural Networks that can generate synthetic data utilized to augment datasets. CGAN employs labels as a condition for a specific class of the generated image among the classes' numbers in the training dataset [23]. CGAN consists of two network generators and discriminator networks. These two networks have opposite learning goals, allowing for a more realistic image. Suppose both the Generator and Discriminator are conditioned with additional information, like class labels. GAN can be expanded to a conditional model [24]. Conditioning can be done by adding the class label  $y$  to the Discriminator and Generator as an extra input layer. CGAN is unsupervised learning. The CGAN block diagram for COVID-19 X-rays image generation used in our experiment shows in Fig. 5.

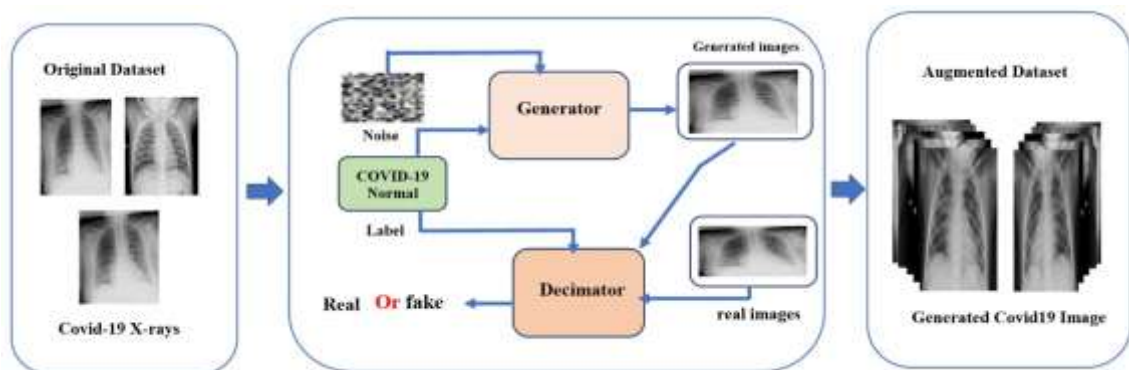


Fig. 5. The Proposed CGAN block diagram for X-rays Image Generation.

A CGAN used two networks: a generator and a discriminator. The two networks have opposite learning goals. The generator produces samples from a latent space and tries to make these samples indistinguishable from the ones contained in the training distribution. Contrarily, the discriminator network tries to infer if the generator generated the samples provided from the training distribution. Both

networks are differentiable and can be trained using the back-propagation algorithm. The discriminator is modified first because it is generally in the lead, and the generator has to learn via the discriminator. In addition, annealing specific instance noise was included in the training to increase gradient flow at the start of the training. CGAN has been trained in the manner of a min-max algorithm. The loss function is similar to a min-max game with two players, as shown by Equation 1 [24].

$$\text{Min}_G \text{max}_D V(\mathbf{D}, \mathbf{G}) = E_{X \sim P_{data}(x)} [\log(d(X|Y))] + E_{z \sim P_g(z)} [\log(1 - D(G(Z|Y)))] \quad (1)$$

Where...

- $D(x|y)$ : denotes the discriminator estimated the probability for the sample of real data.
- $(x)$ : is actuator reality for class  $(y)$ .
- $D(G(z|y))$ : denotes the discriminator estimated the probability for the sample of fake data.

## ii. Generator Network

The generator input is a noise vector of  $n$ -elements sampled from a Normal Gaussian Distribution of the original image. Correspondingly, to generate a batch of images, we need a batch of vectors, which takes 128-dimensional noise vector, and it also needs auxiliary information that tells explicitly the generator which class sample to produce.

The generator takes label  $y$  as COVID-19 class =1 and turns it into a dense vector of size 128 (the length of the random noise vector) by using the Keras embedding layer [25]. Embedding maps an integer into a dense vector of the desired size. We used to embed to create a joint hidden representation from a random noise vector and a label, then combined the label embedding with the noise vector  $z$  into a joint model using the Keras Multiply layer.

This layer multiplies the corresponding entries of the two equal-length vectors ( $128 \times 128$ ) and outputs a single vector of the resulting products (16,384). The resulting vector is used as input into the CGAN. In addition, the images are normalized to be between -1 and 1 (the same range generated by the uniform distribution). The CGAN Generator network consists of five Dense layers. Four hidden Dense layers were normalized by Batch Normalization. They used the leakyReLU activation function, which is like ReLU, but it contains a small amount of slope when it gets from negative values.

We apply and customize combinations of numbers dense layers to enhance the quality of the synthetic generated images. We have improved the hyperparameter set of two networks resulting in the best image quality output. We utilize the Tanh activation function in the last layers, which makes the real value input and outputted in the range -1 to 1 values because we normalize each image from [-1, +1]. Finally, we will input 128-dimensional noise into the network and output a vector of the size 50,176. Later, we will reshape the vector to a matrix with the dimension of ( $224 \times 224 \times 1$ ), the original size of the synthetic images  $x^*|y$ , which passes to discriminator networks as input. The generator is a multi-layer perceptron (MLP) with four hidden layers orders as **128, 256, 512, and 1024** nodes at each layer, the generator loss decreases consistency as the training process and sample quality increase. Fig. 6 show the proposed CGAN Generator architecture.

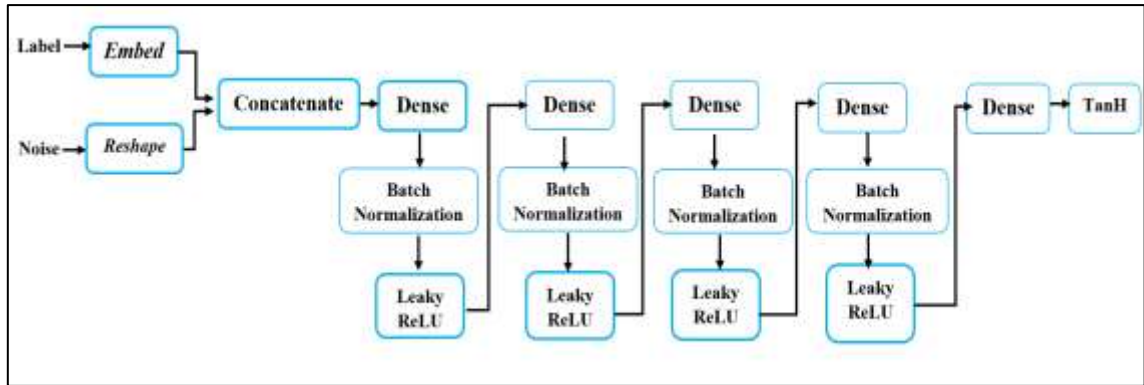


Fig. 6. Proposed CGAN Generator architecture.

iii. Discriminator Network

The Discriminate main task is to get a single probability while predicting real or fake data. The Discriminator is taking both real images from the original dataset with COVID-19 class labels ( $x|y, y$ ), and synthetic images that are generated from the generator phase with COVID-19 class labels ( $x^*|y, y$ ) as input, which takes as input a 50,176-dimensional vector ( $224 \times 224 \times 1$ ). Each original and synthetic image is connected with a class label. The discriminator network consists of five Dense layers; we increase the depth of each hidden Dense layer to 512. The reasoning behind this change is that more information was extracted; this network architecture yielded better results experimentally. The hidden Dense layers are joined by four leakyReLU activation Function layers, a three-patch normalization, and two dropout layers. It is possible to reduce the network’s capacity while training and avoid overfitting.

LeakyRelu is utilized in the generator and discriminator, which helps faster the model's convergence last Dense Layer; applying a sigmoid activation function is essentially a binary classifier to produce a probability incanting whether the input pair is real or synthetic. Finally, the discriminator network is modified for a half batch of actual data and a half batch of synthetic data. The CGAN model modifies the generator. This impact of upgrading the generator to make it better at generating actual samples in the upcoming batch. Fig. 7 shows the CGAN discriminator architecture.

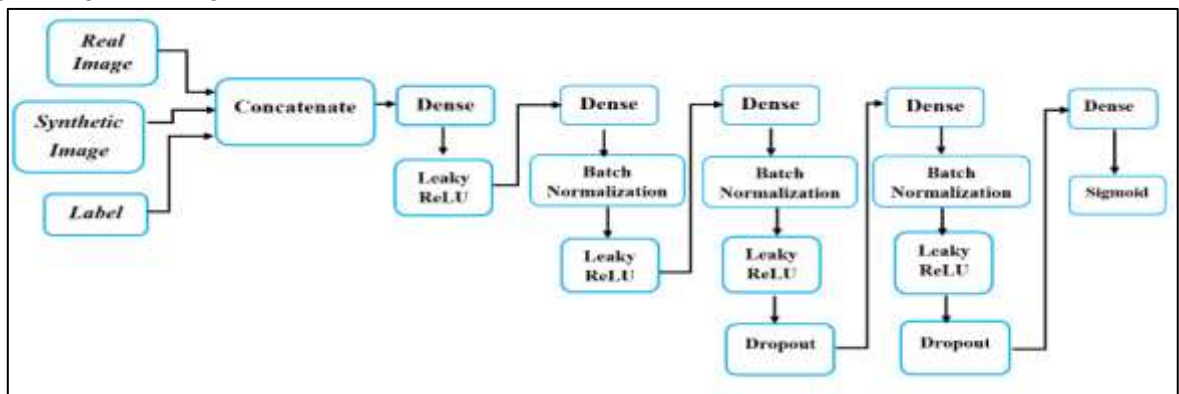


Fig. 7. The proposed CGAN Discriminator architecture.

iv. CGAN Hyper-Parameter

Hyper-parameters are parameters whose values are used to control and regulate the learning process. The adjustment of hyper-parameters has significant improvements in CGAN. Afterward, adjusting some global variables throughout the training CGAN enhances the image resolution quality and reduces the training time. The CGAN hyperparameter as *batch size* defines how many samples are fed into the neural networks at once and sets the buffer size parameter equal to the length of the training data set for perfect

shuffling. The steps will get updated when the training network is learning rate. We have utilized a label binarized to present the labels depending on the classes used. After this CGAN augmentation stage, the whole dataset will be balanced and ready for training and classifying. The initial COVID-19 dataset includes 567 X-ray images each image with a size 224×224.

The number of epochs and batch size used in our experiment are utilized for training the CGAN. The number of epochs was used to determine the image quality. So, after a training epoch, that fuzzy and noisy image was obtained. After many iterations with adjusting the hyper-parameter, we got the best results. Increasing the epochs to (10000), and the batch size to (128). Decreasing the learning rate to (0.0002), which gave a good-resolution synthetic image. The hyperparameters used in CGAN display Table 2.

**Table 2.** The hyperparameters are being used in the CGAN.

Hyperparameters	values
Learning Rate (B1)	0.0002
Learning Rate (B2)	0.6
momentum (alpha)	0.2
momentum (Beta)	0.8
number of epochs	10000
Batch Size	128
Sample interval	200
No Class label	2
<b>Latent Space Size</b>	128
<b>Optimizer</b>	Adam

#### d. Evolution phase

To accurately assess generated image performance, we utilize the image quality metric Frechet inception distance (FID) [26], which has stood out in recent years as a state-of-the-art performance metric in GANs. Although the similarity between sets of images remains an open problem in image processing, FID has been one of the latest heuristics designed to cope with this. This is a metric for evaluating the quality of generated images and was specifically developed to evaluate the performance of GANs.

FID uses the pre-trained Inception-v3 CNN for the feature extraction of the real (x) and synthetic (g) images. Specifically, the coding layer of the CNN (the last pooling layer prior to the output classification of images) is used to capture computer vision-specific features of an input image, thus obtaining a feature vector of 2048 numerical values. This feature space is interpreted as a continuous multivariate Gaussian distribution. Therefore, from the features obtained, it is calculated the Fréchet (also named Wassertein-2) distance between both distributions using their estimated mean ( $\mu$ ) and covariance ( $\Sigma$ ). The lower this metric is, the more similar the two sets of images are, being zero when they are equal [26]. The FID's formula is the following:

$$\text{FID}(x, g) = \|\mu_x - \mu_g\|_2^2 + \text{Tr}(\Sigma_x + \Sigma_g - 2(\Sigma_x \Sigma_g)^{\frac{1}{2}}) \quad (2)$$

Where

$\|\mu_x - \mu_g\|_2^2$  : the sum squared difference between the two mean vectors.

$\text{Tr}(\Sigma_x + \Sigma_g)$ : the sum of the elements along the main diagonal of the square matrix, (the trace linear algebra operation).

$(\Sigma_x \Sigma_g)^{\frac{1}{2}}$ : the square root of the square matrix, given as the product between the two covariance matrices.

#### 4. Experiment Result and Discussion

We implement the proposed method on a Computer Machine supported with Windows 11 Professional-bit operating system, processor 11th Gen Intel(R) Core(TM) i7-1165G7 @2.80GHz 2.80 GHz, and RAM 16.0 GB. This section contains information on the thesis software requirements and the necessity for adequate internet access. The software tools and program language that were used in the implementation of the proposed method are Google Collab, Python, TensorFlow.

The synthetic images which CGAN generates on different epochs, Where the first synthetic image was generated with only 100 epochs, the second generated image 250 epochs, the third generated image 500 epochs up to the last image in Fig. 8 where it was generated with only 10,000 epochs.

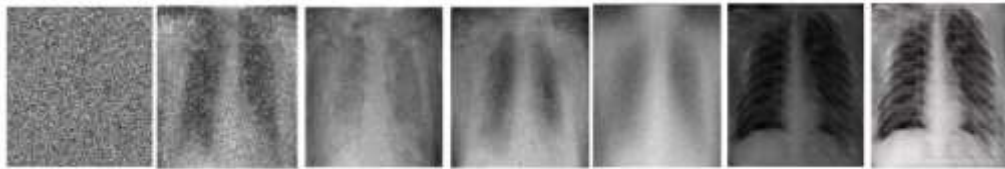


**Fig. 8.** CGAN training to generate synthetic images over different epochs.

In our experiments, CGAN can generate 1200 images for the COVID-19 class. Serval images have some noise, these images were removed. The rest images have good resolution and variety based on the visual turning test. This will help to achieve better improvement in the diagnosis model. The proposed CGAN increases the number of COVID-19 X-rays images to be equal to the amount of X-rays image in the normal class dataset. The initial X-rays images dataset, and the augmented dataset with two classes are listed in Table 3.

**Table 3.** The number of images for each class in the chest X-rays dataset

<i>Dataset</i>	<i>Normal</i>	<i>COVID-19</i>
<b>Original Dataset</b>	1587	567
<b>Original +CGAN Dataset</b>	1587	1587

By using deep dense layers and improving hypermeters with data training up to 10000 epochs. CGAN is able to produce high-resolution images close to the original images, and it outperformed several approaches with CGAN to generate synthetic images. The resolution of this image is especially important in diagnostic models, which are dependent on the quality and resolution of medical images. Fig. 9 shows the resolution of synthetic images compared to the original images in the dataset.

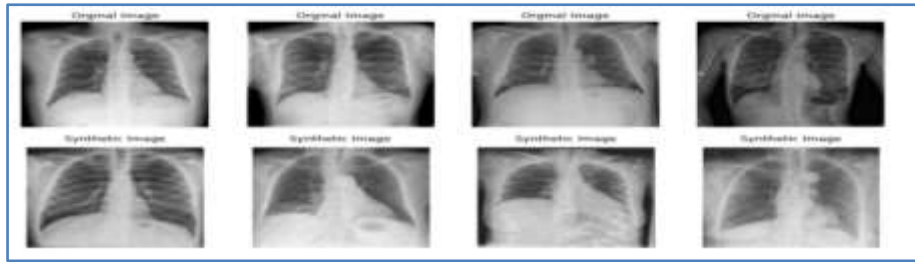


**Fig. 9.** Synthetic images and original images.

Our model can extract the feature of the actual images and collect them in one image. Continuous training can produce various synthetic images. So, the proposed CGAN can generate a new image (unseen images). This is known as diversity in image generation, we prefer CGAN over traditional techniques due to generating unseen images; it is prepared like art. Thus, our model has outperformed the traditional methods of augmentation which in turn cannot generate new images but only make some transformations to the same image. Fig. 10 shows a synthetic image that combines the features of two real images from the original dataset. Fig. 11 shows a diversity of the generated images.



**Fig. 10.** CGAN generates unseen images.

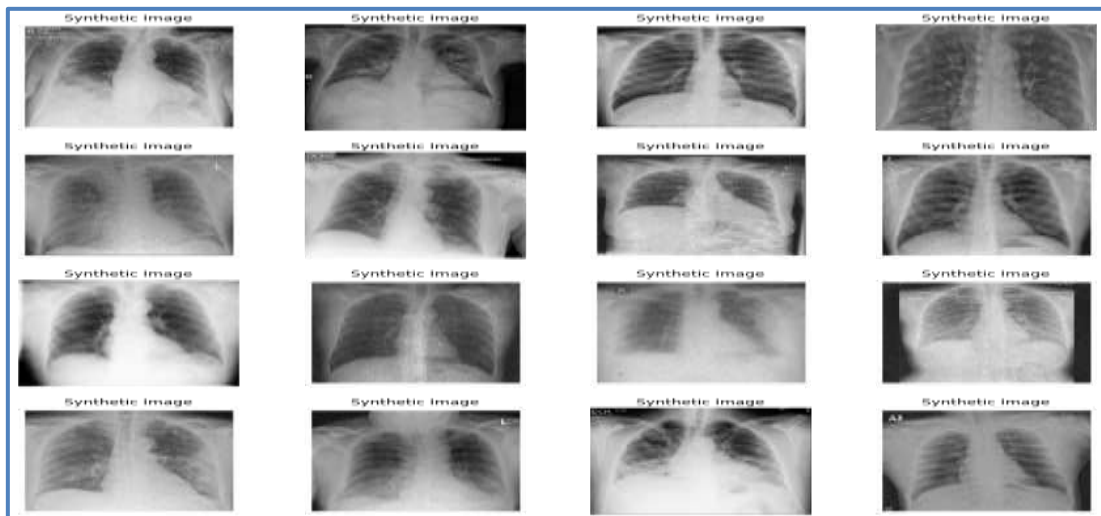


**Fig. 11.** Sample of synthetic COVID-19 X-rays images.

### 5. Comparative Analysis

The experiments of the proposed model and other methodologies are presented in this section, Table 4 comparison between the proposed model and previously reviewed models depending on the FID metric.

**Table 4.** Image quality evaluation results of synthetic images ( $\downarrow$  indicates a lower number is better.)

Other Study	DataSet Type	Method	FID $\downarrow$
Likun Cai et al.[13]	MNIST, SVHN, and CeLebA	Alpha-GAN	176.37,23.26
Berezsky et al.[14]	X-rays	CDCGAN-PSO	2.988
Shmelkov et al. [15]	CIFAR10, CIFAR100	SNGAN,WGAN(10M) , WGAN (2.5 M), DCGAN	11.8, 14.1, 15.0, 35.6
shuang et al.[16]	X-rays	SAGAN	30.55
Waheed et al. [17]	X-rays	ACGAN	4.296
Loey et al. [18]	X-rays	GAN	5.846
<b>proposed model</b>	<b>X-rays</b>	<b>CGAN</b>	<b>2.349</b>

Table 4 presents the FID evaluation of the synthetic images obtained from CGAN generators and compares them with the state-of-the-art GANs in synthesis images, as well as with the random creation of GANs. This table contains the implemented GAN model as well as its average FID obtained from comparing the results of each model with the CGAN. As can be seen in the aforementioned table, the results obtained through the evolution of GAN architectures with progressive training improved the results of previous works in the synthetic images, showing that the networks obtained by the proposed method have a better average (lower) in the FID evaluation values than the rest of the works. The promising results are an indication of the potential for improvement that CGAN can offer to obtain better trained GANs and then with better quality in their results. Our proposed CGAN model in addition to the high resolution of image generation also generates high diversity of new images due to the deep dense layers and improving hyperparameters with training data. improvement of the hyperparameters used as the learning rate and depth of networks used in generation and classification; As a result, CGAN can produce high-resolution images close to the original images, and it outperformed several approaches with GAN to generate synthetic images. The augmented dataset is balanced as the data in each category converge.

## 6. Conclusions

The widespread scope of coronavirus (COVID-19) adversely affected healthcare systems. Medical images, such as X-ray images, are used to determine COVID-19 infection. However, the main problem in medical images is the limited dataset that is used to train in the DL models. Adjusted CGAN to generate synthetic COVID-19 X-ray images similar to the original image, which generate high-resolution and variety images when compared to common image synthesis approaches. After applying the adjusted CGAN the dataset conation the process of augmentation of the COVID-19 dataset was able to balance the COVID-19 and normal classes in the dataset, each class content 1587 images and thus solve the problem of overfitting, the augmented dataset became suitable for training and obtaining reliable results our CGAN generate synthetic images with high resolution and a wide variety, CGAN model takes only 2 hours,48 minutes, and 6 seconds to accomplish the run. The experimentation carried out also verified the high quality of the synthetic images verified by their low FID values. In future work, we would like to work on the mechanism of medical data transmission over Wi-Fi between both the server-side and

client-side to design a web system based on the medical diagnosis model and dataset to provide more help to the doctors in their diagnoses.

## References

- [1] Y.M.Y. Abdallah, T. Alqahtani, *Medical Imaging-Principles and Applications 1* (2019).
- [2] W.C. Serena Low, J.H. Chuah, *Computational and Mathematical Methods in Medicine* **2021**, (2021).
- [3] L. Chang, Y. Yan, L. Wang, in *Transfusion medicine reviews* **34** (2), 75 (2020).
- [4] T. Higaki, Y. Nakamura, J. Zhou, Z. Yu, T. Nemoto, F. Tatsugami, K. Awai, *Academic radiology* **27**(1), 82 (2020).
- [5] T. Iqbal, H. Ali, *Journal of Medical Systems* **1**, 1 (2018).
- [6] X. Yi, E. Walia, P. Babyn, *Medical image analysis* **58**, 101552 (2019).
- [7] H.P. Das, R. Tran, J. Singh, X. Yue, G. Tison, A. Sangiovanni-Vincentelli, C.J. Spanos, *Proceedings of the AAAI Conference on Artificial Intelligence* **36**(11), 11792 (2022).
- [8] J. Ker, L. Wang, J. Rao, T. Lim, *IEEE Acces*, **6**, 9375 (2017).
- [9] I. Goodfellow, J. Pouget-Abadie, M. Mirza, B. Xu, D. Warde-Farley, S. Ozair, A. Courville, Y. Bengio, *Communications of the ACM* **63**(11), 139 (2020).
- [10] N. Aldausari, A. Sowmya, N. Marcus, G. Mohammadi, *ACM Computing Surveys (CSUR)* **55**(2), 1 (2022).
- [11] S. Kazemina, C. Baur, A. Kuijper, B. van Ginneken, N. Navab, S. Albarqouni, A. Mukhopadhyay, *Artificial Intelligence in Medicine* **109**(1), 101938 (2020).
- [12] A.B. Levine, J. Peng, D. Farnell, M. Nursey, Y. Wang, J.R. Naso, H. Ren, H. Farahani, C. Chen, D. Chiu, A. Talhouk, *The Journal of pathology* **252**(2), 178 (2020).
- [13] L. Cai, Y. Chen, N. Cai, W. Cheng, H. Wang, *Entropy* **22**(4), 410 (2020).
- [14] O.M. Berezsky, P.B. Liashchynskyi, *Applied Aspects of Information Technology* **4**(3) 250 (2021).
- [15] K. Shmelkov, C.Schmid, K.Alahari, *Proceedings of the European conference on computer vision (ECCV)*, 213 (2018).
- [16] D. shuang Li, X. bing Hu, H. gang Zhang, J. feng Yang, *Optoelectronics Letters* **17**(2), 112 (2021).
- [17] A. Waheed, M. Goyal, D. Gupta, A. Khanna, F. Al-Turjman, P.R. Pinheiro, *IEEE Access* **8**, 91916 (2020).
- [18] M. Loey, F. Smarandache, N.E.M. Khalifa, *Symmetry* **12**(4), 651 (2020).
- [19] J.P. Cohen, P. Morrison, M. Ghassemi, *Journal of Machine Learning for Biomedical Imaging* **2020**(2), 1 (2020).
- [20] L. Wang, Z.Q. Lin, A. Wong, *Scientific Reports* **10**, 1 (2020).
- [21] D.S. Kermany, M. Goldbaum, W. Cai, C.C. Valentim, H. Liang, S.L. Baxter, A. McKeown, G. Yang, X. Wu, F. Yan, Dong, *Cell*, **172**(5), 1122 (2018).
- [22] C. Shorten, T.M. Khoshgoftaar, *Journal of big data* **6**(1), 1 (2019).
- [23] H. Majid, K. Ali, *Iraqi Journal for Electrical and Electronic Engineering* **18**(1), 103 (2022).
- [24] J.A. Rodríguez de la Cruz, H.G. Acosta Mesa, E. Mezura Montes, F. Arámbula Cosío, B. Escalante Ramírez, J. Olveres Montiel, *17th International Symposium on Medical Information Processing and Analysis* **12088**, 85 (2021).
- [25] R. Rahutomo, A.S. Perbangsa, H. Soeparno, B. Pardamean, *2019 International Conference on Information Management and Technology (ICIMTech)* **1**, 537 (2019).
- [26] M. Heusel, H. Ramsauer, T. Unterthiner, B. Nessler, S. Hochreiter, *Advances in neural information processing systems* **30**, 6627 (2017).

## توليد صور الأشعة السينية للصدر عالية الدقة باستخدام شبكات الخصومة التوليدية المشروط

حنين ماجد محمد\* ، خولة حسين علي

قسم علوم الحاسوب، كلية التربية للعلوم الصرفة، جامعة البصرة، البصرة، العراق.

### المخلص

### معلومات البحث

تفوقت نماذج التعلم العميق (DL) بشكل ملحوظ وفعال على العديد من تطبيقات رؤية أجهزة الكمبيوتر. ومع ذلك، تتطلب هذه النماذج كميات كبيرة من البيانات لتجنب المشكلات المفرطة. يحدث التجهيز الزائد عندما تقوم الشبكة بتدريب وظيفة ذات تباين كبير لتمثيل بيانات التدريب بشكل مثالي. وبالتالي، تفترق الصور الطبية إلى توافر مجموعات بيانات كبيرة تحمل علامات، كما أن شرح الصور الطبية مكلف ويستغرق وقتاً طويلاً بالنسبة للخبراء، نظراً لأن فيروس COVID-19 مرض معدٍ، وهذه مجموعات البيانات نادرة ومن الصعب الحصول على مجموعات بيانات كبيرة.

الكمية المحدودة من فئة COVID-19 مقارنة بأي فئات أخرى، على سبيل المثال (صحية). لحل مشكلة ندرة البيانات، نقوم بتعديل شبكة الخصومة التوليدية المشروطة (CGAN) كحل لمشاكل الندرة والبيانات المحدودة. يحتوي CGAN على شبكتين عصبيتين: مولد يخلق صوراً اصطناعية (مزيفة)، ومميز يتعرف على عينة حقيقية من التدريب وعينة مولدة من المولد. CGAN المعدلة قادرة على إنشاء صور اصطناعية بدقة عالية وقريبة من الصور الأصلية التي تساعد في توسيع مجموعة البيانات المحدودة الخاصة بالجائحة الجديدة. بالإضافة إلى استراتيجيات تعزيز CGAN، يستكشف هذا البحث أيضاً لفترة وجيزة جوانب إضافية لزيادة البيانات مثل الوقت المستغرق وحجم مجموعة البيانات الإجمالي. تم استخدام Frechet مقياس مسافة بدء التشغيل (FID) لتقييم الصور الاصطناعية التي تم إنشاؤها بواسطة CGAN. تحصل CGAN المعدلة على نتائج FID أفضل لصور الأشعة السينية الاصطناعية عالية الدقة التي تحققها بنسبة 2.349٪.

الاستلام 05 آب 2022  
القبول 21 ايلول 2022  
النشر 30 كانون الاول 2022

### الكلمات المفتاحية

كوفيد-19، شبكات الخصومة التوليدية، شبكات الخصومة التوليدية المشروطة صور اصطناعية.

**Citation:** H.M. Mohammed, K.H. Ali, J. Basrah Res. (Sci.) 48(2), 88 (2022).  
[DOI:https://doi.org/10.56714/bjrs.48.2.9](https://doi.org/10.56714/bjrs.48.2.9)

\*Corresponding author email : [hneenaltmemi@gmail.com](mailto:hneenaltmemi@gmail.com)

